Supporting Information

Efficient Charge-Transfer from Diketopyrrolopyrroles to Single-Walled Carbon Nanotubes

Ilias Papadopoulos,‡[a] Arjun Menon,‡[a] Fabian Plass,[a,b] Desiré Molina,[c] Christina Harreiß,[d] Axel Kahnt,[b] Erdmann Spiecker,[d] Ángela Sastre-Santos,*[c] and Dirk M. Guldi*[a]

[a]*Department of Chemistry and Pharmacy & Interdisciplinary Center for Molecular Materials (ICMM) , Friedrich-Alexander-University Erlangen-Nuremberg, Egerlandstraße 3, 91058 Erlangen, Germany. E-mail: dirk.guldi@fau.de (D.M.G.)*

[b]*Leibniz Institute of Surface Engineering (IOM), 04318 Leipzig, Germany.*

[c]*Área de Química Orgánica, Instituto de Bioingeniería, Universidad Miguel Hernández, Avda. de la Universidad s/n, 03203 Elche, Spain. E-mail: asastre@umh.es (Á.S.-S.)*

[d]*Institute of Micro- and Nanostructure Research (IMN) & Center for Nanoanalysis and Electron Microscopy (CENEM) and Interdisciplinary Center for Nanostructured Films (IZNF), Friedrich-Alexander University Erlangen-Nuremberg, Cauerstraße 3, 91058 Erlangen, Germany.*

‡ These authors contributed equally to this work.

General Procedures, Materials, and Methods

Materials

All the chemicals and materials were purchased and used as received unless otherwise noted. Column chromatography was performed with SiO_2 (40–63 μm), and TLC plates coated with SiO_2 60F254 were visualized by UV light. SWCNTs with a broad chirality range (0.7−1.3 nm in diameter, >77% of carbon as SWCNT) were purchased from Sigma- Aldrich and used as obtained. Tetrahydrofuran of HPLC quality (>99.9%) was used as purchased from ROTH.

General Procedure for Dispersion Preparation of SWCNTs and DPP/SWCNT

SWCNTs -: 0.1 mg of SWCNTs were suspended in THF (4 mL) by sonication for 20 min, followed by 10 min of centrifugation at 5000 g and subsequent sonication for 3 min.

DPP-Ph/SWCNT and **DPP-PhBr/SWCNT** -: 0.1 mg of SWCNTs and 2 x 10^{-5} M (**DPP-Ph** and **DPP-PhBr**) were suspended in THF (4 mL) by sonication for 20 min, followed by 10 min of centrifugation at 5000 g and subsequent sonication for 3 min.

DPP-Th/SWCNT -: 0.1 mg of SWCNTs and 1 x 10^{-5} M (**DPP-Th**) were suspended in THF (4 mL) by sonication for 20 min, followed by 10 min of centrifugation at 5000 g and subsequent sonication for 3 min.

Characterization

Spectroscopy

UV−vis−NIR absorption spectra were measured using a Cary 5000 spectrometer (Varian) and 10 × 10 mm quartz cuvettes. NIR individual spectra and photoluminescence excitation (PLE) intensity maps were obtained with a FluoroLog 3 spectrometer from Horiba Yobin Yvon using a 450 W xenon lamp and a Symphony InGaAs array in combination with an iHR320 imaging spectrometer. A Fluoromax 3 spectrometer from Horiba Yobin Yvon was used for fluorescence and 3D fluorescence measurements in the visible region. Femtosecond transient absorption measurements were performed with the transient absorption pump probe system HELIOS from Ultrafast Systems. Laser pulses with a pulse width of 150 fs were performed with a CPA-2110 titanium:sapphire laser system from Clark-MXR Inc. (output 775 nm, 1 kHz). The 550 nm excitation pulses were generated by using a noncollinear optical parametric amplifier (NOPA, Clark MXR). OS quartz cuvettes of 2 mm were used for all pump probe measurements. Transient absorption data were evaluated by means of multiwavelength and target analysis using the GloTarAn software, utilizing the proposed kinetic model. The analytic solution to the coupled differential equations that describe the kinetic model is convoluted with a Gaussian instrument response function. After the least-squares fitting has converged, the raw

data matrix is deconvoluted using the specific solution to the kinetic model and parameters from the fit to obtain the species-associated spectra and their populations as a function of time. NMR spectra were recorded at 25°C with a Bruker AC300 spectrometer. The solvents for spectroscopic studies were spectroscopic grade and were used as received. UV-vis spectra in chloroform solution were measured with a Helios Gamma spectrophotometer and the extinction coefficients were calculated using the Lambert-Beer Law. IR spectra were measured with a Nicolet Impact 400D spectrophotometer. High-resolution mass spectra were obtained with a Bruker Microflex LRF20 matrix-assisted laser desorption/ionization time of flight (MALDI-TOF) spectrometer using dithranol as matrix.

Raman Spectroscopy/Microscopy

Raman measurements were performed with a WiTec alpha300r confocal Raman microscope. A HeNe laser with an output of 633 nm was used for sample excitation.

Microscopy

Transmission electron microscopy (TEM) was carried out with an aberration-corrected Titan Themis 300 (FEI Company, Hillsboro, OR, USA) equipped with a high-brightness field-emission gun (X-FEG) operated at an acceleration voltage of 80 kV to reduce structural damage. The HRTEM images were obtained employing a FEI Ceta 16 M 4K CMOS camera. The TEM samples were prepared by dropping the SWCNT-containing dispersion onto TEM grids (ultrathin carbon film on a holey carbon support, Ted Pella, Inc.). The height profiles were generated by using the Gatan Microscopy Suite Software GMS 3. AFM measurements were carried out with a JPK Nanowizard 4 Nanoscience microscope holding an ACTA cantilever from Applied Nanostructures APPNANO with a resonance frequency of 300 kHz and a tip radius below 10 nm. Samples were drop-casted onto silica wafers.

Pulse Radiolysis

The DPP samples were irradiated in N_2 saturated butyl chloride (n-BuCl) solutions with high-energy electron pulses (10 MeV, 15 ns duration) by a LINAC-type electron accelerator ELEKTRONIKA-U003 (Toriy, Moscow). The dose delivered per pulse was measured by electron dosimetry,[1] and doses of 85 Gy / pulse were selected. The optical detection of the transients was carried out with a system consisting of a pulsed 1000W xenon lamp (Osram, XBO1000), a Suprasil cell (light path 1 cm), high-intensity grating monochromator (Acton research, SP500), R928 photomultiplier (Hamamatsu Photonics), or a fast InGaAs photodiode and a digital oscilloscope (Tektronix, TDS5034B). A more detailed description on the pulse radiolysis measurements is given in the supporting information.

Synthesis and Characterization

Scheme S1. Synthesis of **DPP-PhBr**, **DPP-Ph**, and **DPP-Th**.

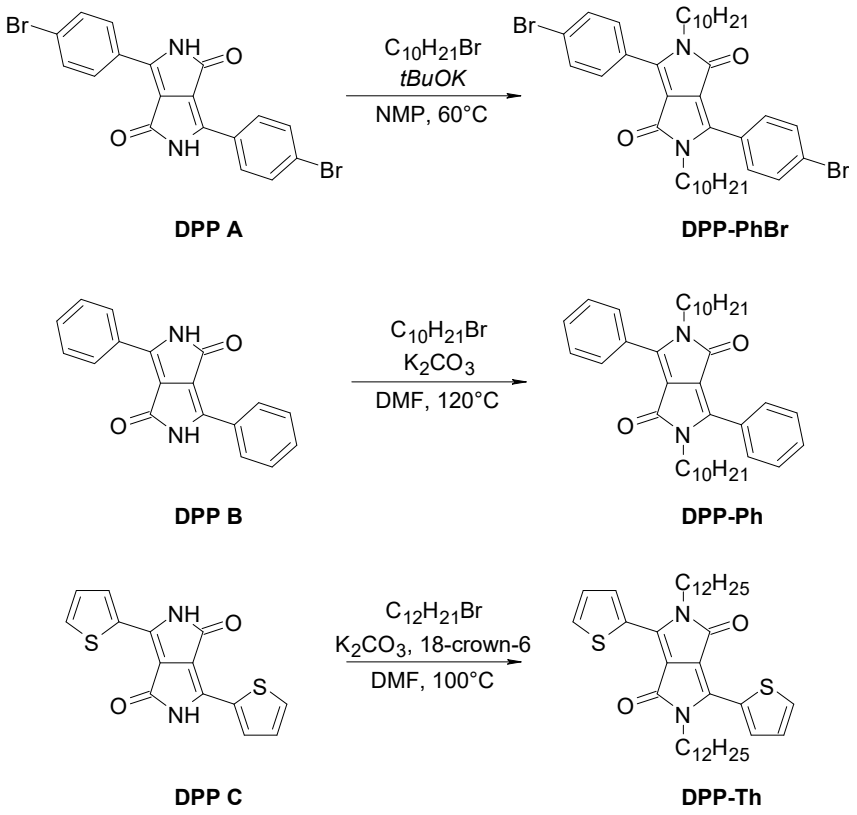

3,6-bis(4-bromophenyl)-2,5-didecyl-2,5-dihydropyrrolo[3,4-c]pyrrole-1,4-dione (DPP-PhBr)

3,6-bis(4-bromophenyl)-2,5-dihydro-pyrrolo[3,4-*c*]pyrrole-1,4-dione (3 g, 6.7 mmol) was mixed with potassium *tert*-butoxide (1.7 g, 15 mmol) in NMP (51 mL) and the temperature was raised to 60°C. 1-Bromodecane was then added dropwise and left at 60°C for 18h. After reaching room temperature, the reaction crude was washed with water, 0.5 M HCl, Brine and extracting with ethyl acetate. The solvent was removed, and methanol added, allowing the product to precipitate. The precipitate was filtered, and the product was purified by chromatographic column using chloroform as eluent. Finally, **DPP-PhBr** was crystallized with methanol/acetone 1:2 to obtain fluorescent-orange crystals with a 45% yield. ^{1}H RMN: (400 MHz, $CDCl_3$) δ = 7.66 (d, *J* = 3.1 Hz, 8H), 3.71 (t, *J* = 7.6 Hz, 4H), 1.54 (m, 4H), 1.29-1.18 (m, 28H), 0.87 (t, *J* = 6.9 Hz, 6H). ^{13}C RMN: (300 MHz, $CDCl_3$) δ = 14.2, 22.8, 26,8, 29.1, 29.4, 29.5, 29.5, 29.6, 32.0, 110.1, 125.9, 127.1, 130.3, 132.3, 147.5, 162.5. UV-Vis (CH_2Cl_2) $\lambda_{max/nm}$ (log ε) = 276 (4.56), 478 (4.35). HRMS (MALDI-TOF) m/z: calc. for $C_{38}H_{50}Br_2N2O_4$ (M), 726.222; found; 726.194. FT-IR (KBr), *v* (cm^{-1}): 2963 (v_A CH_3), 2913 (v_A CH_2), 2870 (v_S CH_3),2849 (v_S CH_2), 1680, 1657 (C=O lactam), 1585, 1554, 1488, 1469, 1440, 1407, 1374, 1300 (C-N), 733 (rocking γ CH_2).

2,5-didecyl-3,6-diphenyl-2,5-dihydropyrrolo[3,4-c]pyrrole-1,4-dione (DPP-Ph)

A solution of 3,6-diphenyl-2,5-dihydropyrrolo[3,4-*c*]pyrrole-1,4-dione (500 mg, 1.7 mmol) and potassium carbonate (2.6 g, 19.1 mmol) in 31 mL of DMF was heated and stirred at 120°C under argon. Then, another solution of 1-bromodecane in 14 mL of DMF was added dropwise, maintaining the temperature for 2 hours after the addition. After reaching room temperature, distilled water was added and filtered. Finally, the solid was crystallized with a 2:1 ethanol/acetone mixture, yielding light orange crystals (31%). ^{1}H RMN: (300 MHz, $CDCl_3$) δ = 7.83 – 7.78 (m, 4H), 7.57-7.50 (m, 6H), 3.79-3.71 (m, 4H), 1.65-1.55 (m, 4H), 1.32-1.15 (m, 28H), 0.87 (dd, J_1 = 8.9 Hz, J_2 = 4.7 Hz, 6H).

2,5-didodecyl-3,6-di(thiophen-2-yl)-2,5-dihydropyrrolo[3,4-c]pyrrole-1,4-dione (DPP-Th)

In a round bottom flask, 3,6-di(thiophen-2-yl)-2,5-dihydropyrrolo[3,4-*c*]pyrrole-1,4-dione (1.0 g, 3.4 mmol), K_2CO_3 (2.0 g) and 18-crown-6 (120.0 mg) were introduced and an argon atmosphere was made. Then dry DMF (12 mL) was injected and the temperature was raised to 100°C. Next, 1-bromododecane (2.6 g, 10.4 mmol) was added dropwise, as slowly as possible. After 24 hours of reaction at the same temperature, the crude was allowed to cool down, washed 6 times with 1M HCl and extracted with ethyl acetate. **DPP-Th** was purified with chromatographic column of toluene and crystallized with methanol, obtaining a spongy maroon solid. Yield: 32%; ^{1}H RMN: (300 MHz, $CDCl_3$) δ = 8.93 (dd, J_1 = 1.1 Hz, J_2 = 3.9 Hz, 2H), 7.64 (dd, J_1 = 1.1 Hz, J_2 = 5.0 Hz, 2H), 7.28 (dd, J_1 = 5.0 Hz, J_2 = 3.9 Hz, 2H), 4.04 (m, 4H), 1.74 (m, 4H), 1.25 (m, 36H), 0.87 (m, 6H).

Figure S1. Comparison between DPP derivatives under normal light and irradiated with λ = 365 nm in solid state.

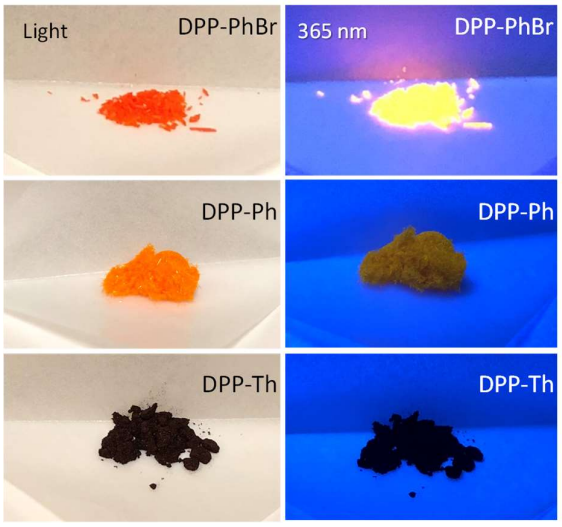

Figure S2. ^{1}H-RMN (25°C, $CDCl_3$) of DPP-PhBr.

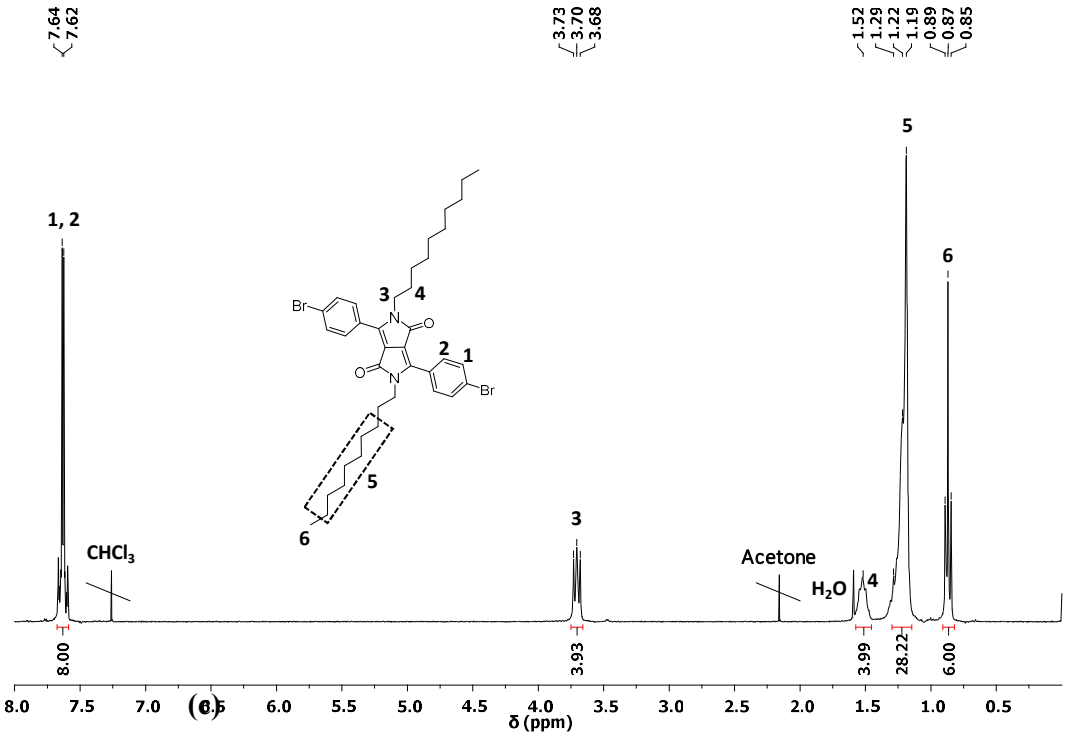

Figure S3. ^{13}C-RMN (25°C, $CDCl_3$) of **DPP-PhBr**.

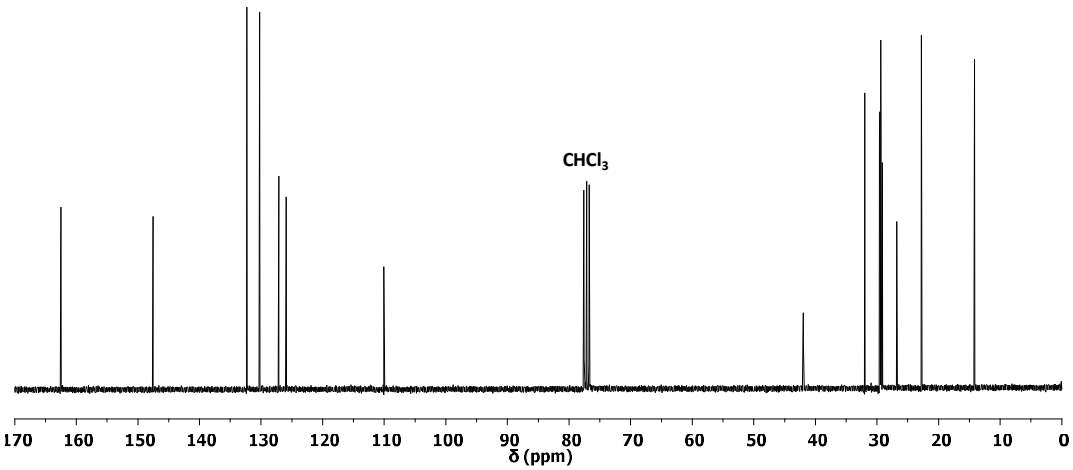

Figure S4. MALDI-TOF spectrum of **DPP-PhBr** (M^+). a) Experimental and b) theoretical spectra.

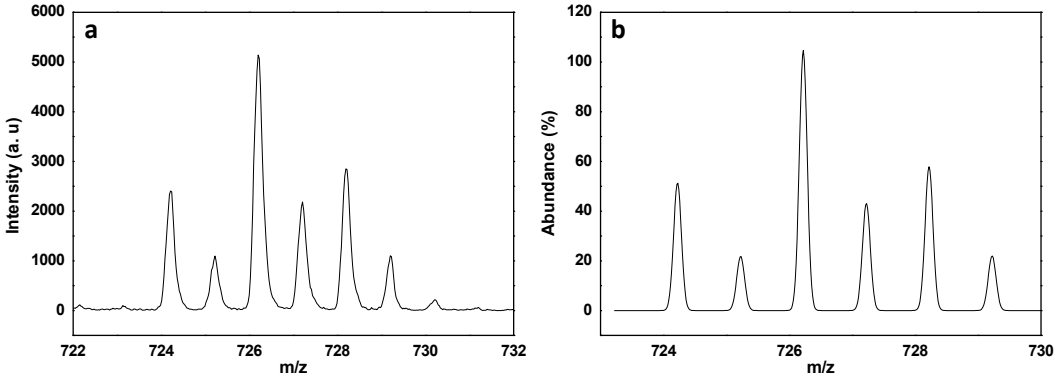

Figure S5. 3D fluorescence heat maps in the visible range of a) **DPP-Ph** (left) and **DPP-Ph/SWCNT** (right), b) **DPP-PhBr** (left) and **DPP-PhBr/SWCNT** (right), and c) **DPP-Th** (left) and **DPP-Th/SWCNT** (right) in room temperature THF with matching absorptions in the 300 to 700 nm photoexcitation range.

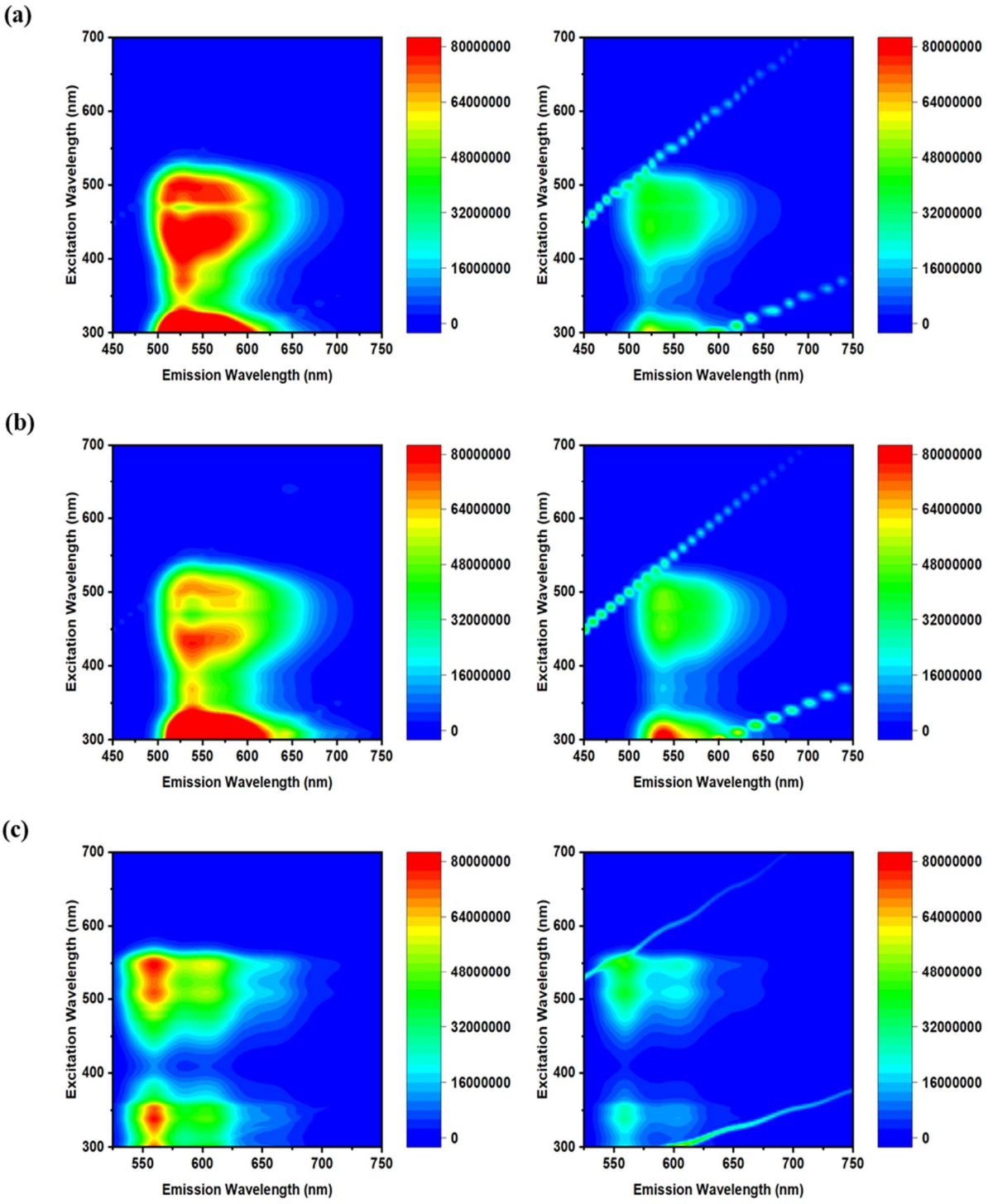

Figure S6. Fluorescence spectra in the visible range of a) **DPP-Ph** (cyan) and **DPP-Ph/SWCNT** (red), b) **DPP-PhBr** (green) and **DPP-PhBr/SWCNT** (blue), and c) **DPP-Th** (violet) and **DPP-Th/SWCNT** (pink) in room temperature THF with matching absorptions at the photoexcitation wavelengths of 430 and 505 nm, respectively.

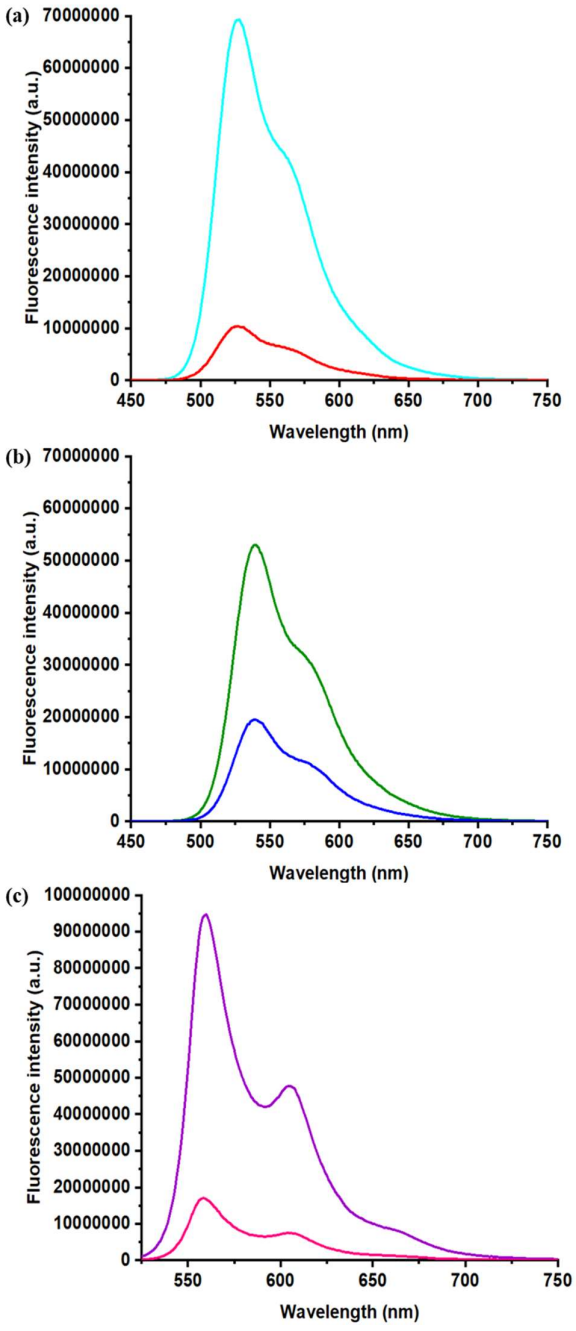

Figure S7. 3D fluorescence heat maps in the near-infrared range of a) **DPP-PhBr/SWCNT** and b) **DPP-Th/SWCNT** in room temperature THF with matching absorptions in the 525 to 800 nm photoexcitation range.

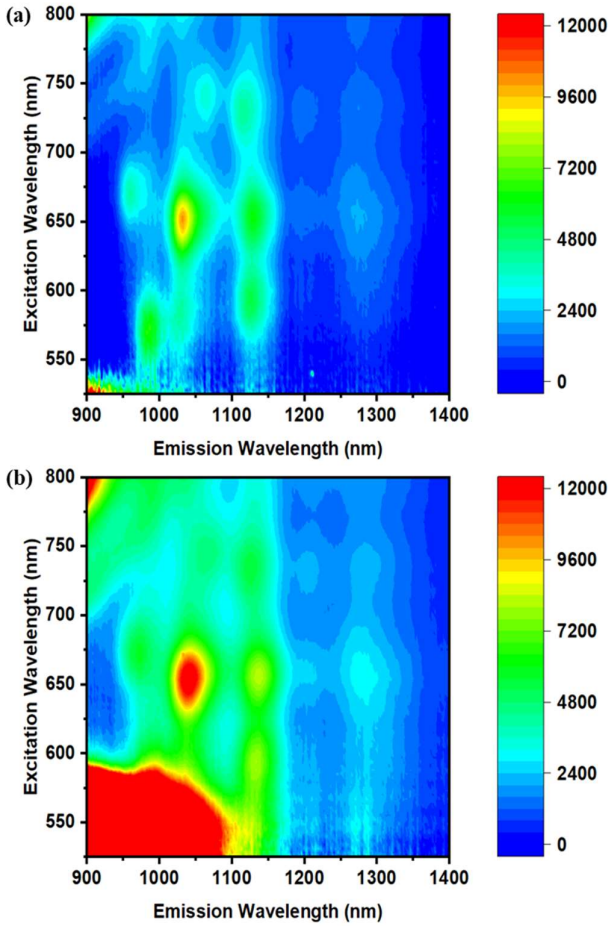

Figure S8. Fluorescence spectra in the near-infrared range of SWCNT (black) and **DPP-Ph/SWCNT** (red), **DPP-PhBr/SWCNT** (blue), and **DPP-Th/SWCNT** (pink) in room temperature THF with matching absorptions at the photoexcitation wavelengths of a) 570 and b) 660 nm.

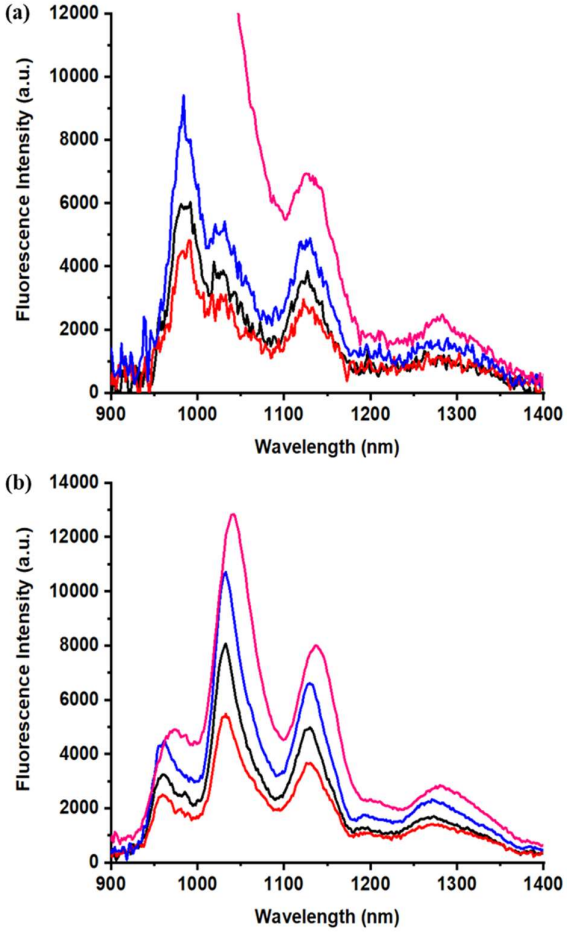

Figure S9. Raman histograms of a) G-mode, b) D-mode, and c) 2D-mode of SWCNT (black), **DPP-PhBr/SWCNT** (blue), and **DPP-Th/SWCNT** (pink) on silicon wafers, which were prepared by drop-casting suspensions of THF. The laser excitation wavelength was 633 nm.

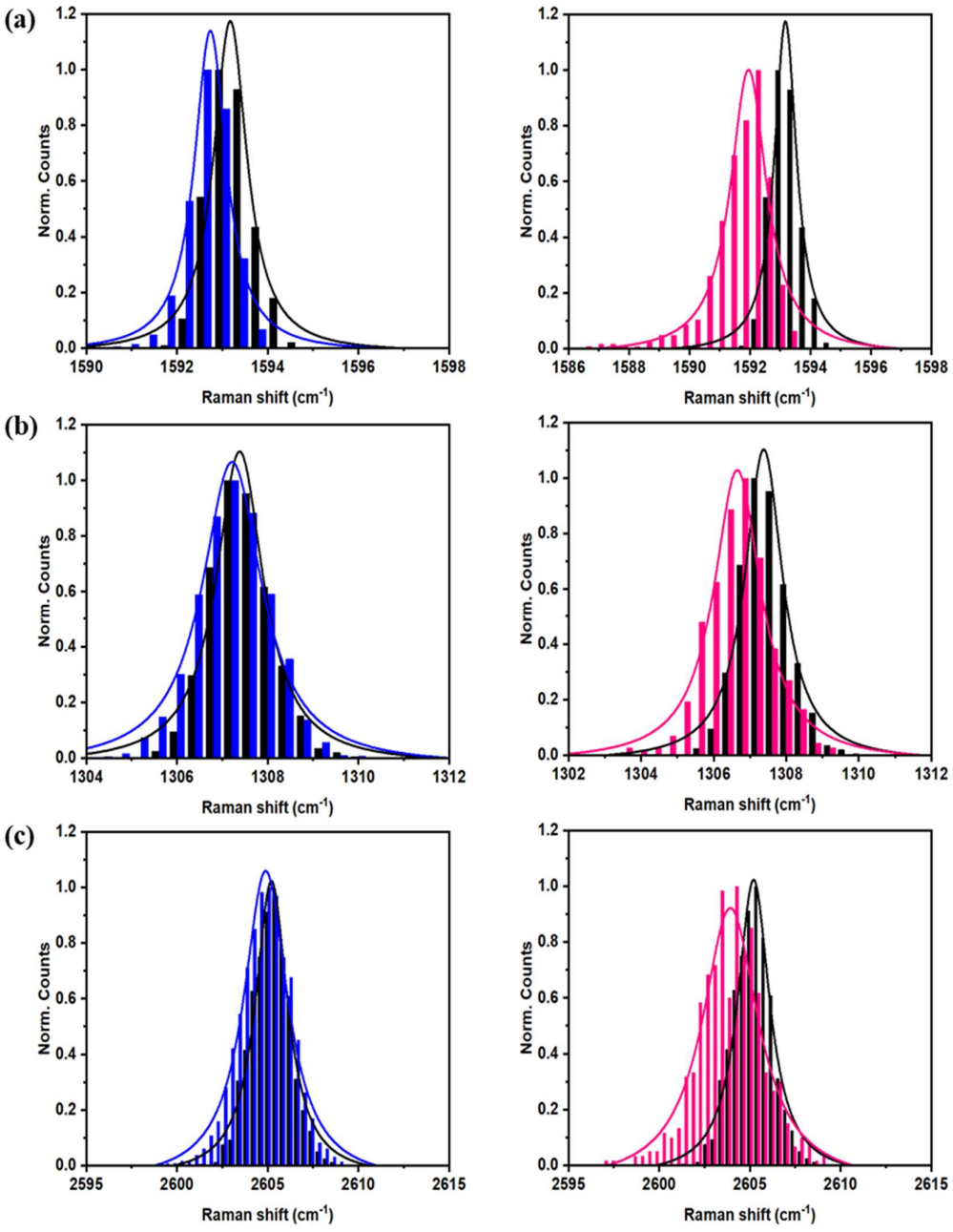

Figure S10. Normalized Raman mean spectra (D-, G-, and 2D-mode) of a) SWCNTs (black) and **DPP-Ph/SWCNT** (red), b) SWCNTs (black) and **DPP-PhBr/SWCNT** (blue), and c) SWCNTs (black) and **DPP-Th/SWCNT** (pink) on silicon wafers, which were prepared by drop-casting suspensions of THF. The laser excitation wavelength was 633 nm.

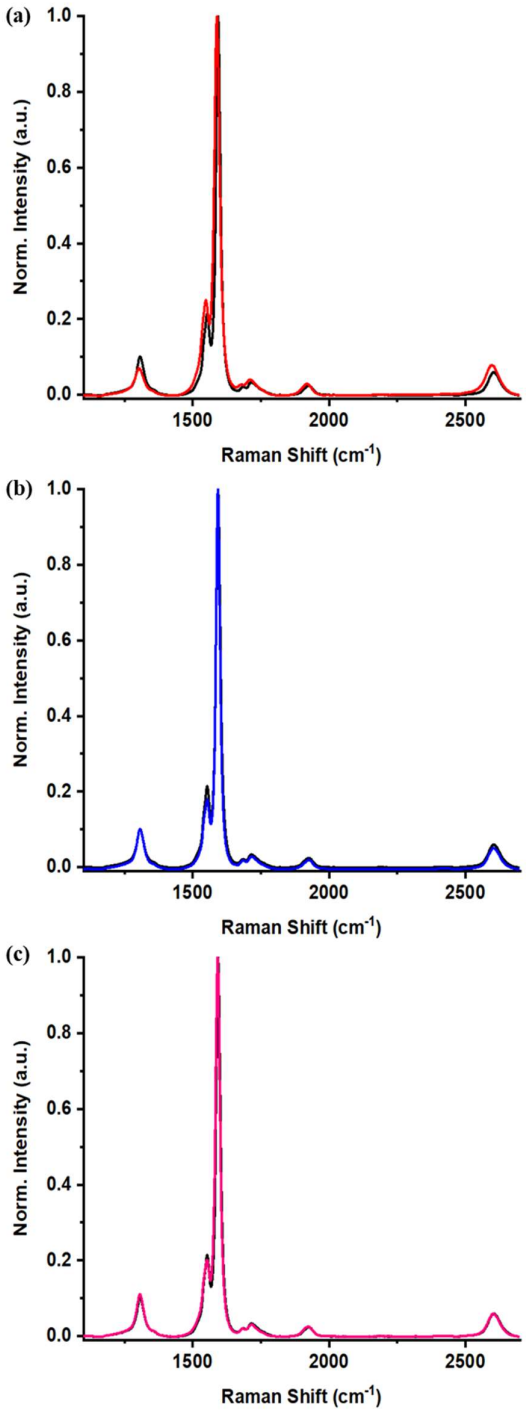

Figure S11. Fs-TAS (0 – 5.5 ns) of SWCNTs in THF at room temperature: a) 3D fs-TAS obtained upon pump probe experiments following 430 nm laser excitation, b) respective time absorption profiles at the given wavelengths, c) deconvoluted fs-TAS spectra of the SWCNT-related singlet excited states stemming from multiple exciton generations $(S_1)_{NT1}$ (blue), interband-intertube relaxations $(S_1)_{NT2}$ (green), and radiative exciton recombination $(S_1)_{NT3}$ (brown) as obtained by target analysis, and d) respective population kinetics.

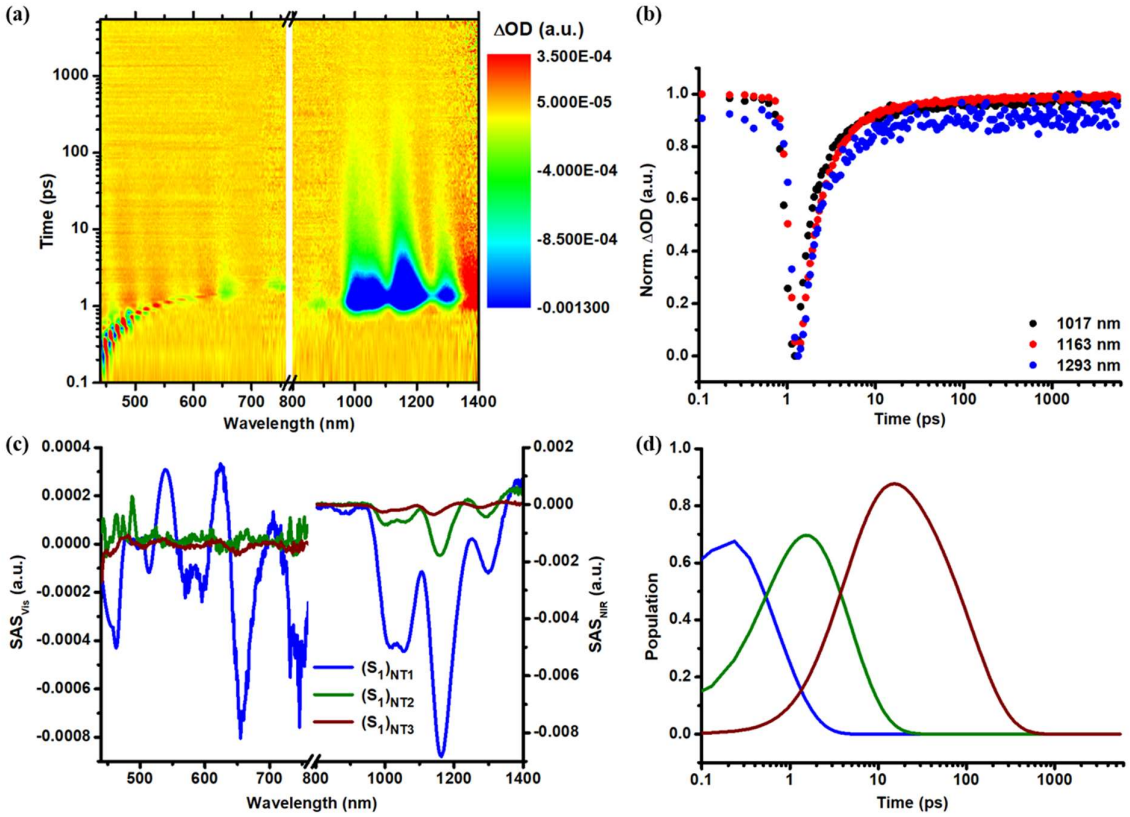

Figure S12. Fs-TAS (0 – 5.5 ns) of SWCNTs in THF at room temperature: a) 3D fs-TAS obtained upon pump probe experiments following 505 nm laser excitation, b) respective time absorption profiles at the given wavelengths, c) deconvoluted fs-TAS spectra of the SWCNT-related singlet excited states stemming from multiple exciton generations $(S_1)_{NT1}$ (blue), interband-intertube relaxations $(S_1)_{NT2}$ (green), and radiative exciton recombination $(S_1)_{NT3}$ (brown) as obtained by target analysis, and d) respective population kinetics.

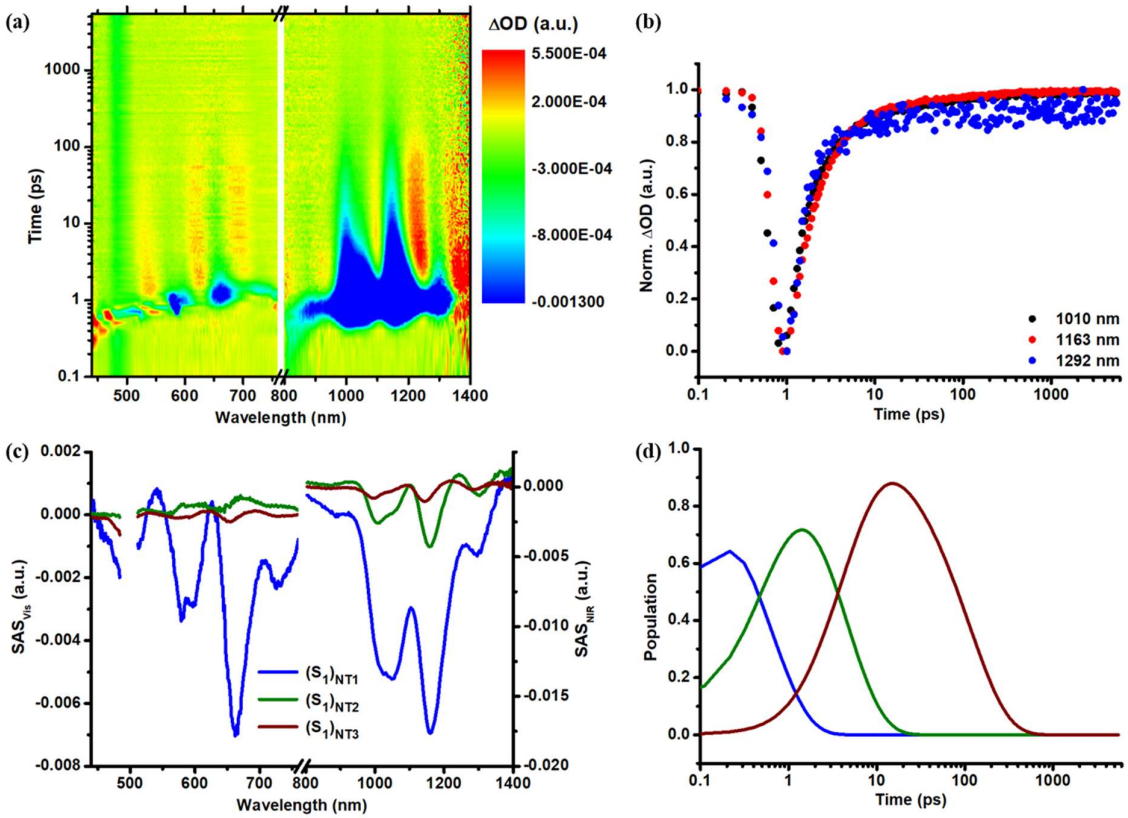

Figure S13. Kinetic model used to fit the transient absorption raw data for **DPP-Ph**, **DPP-PhBr**, and **DPP-Th**.

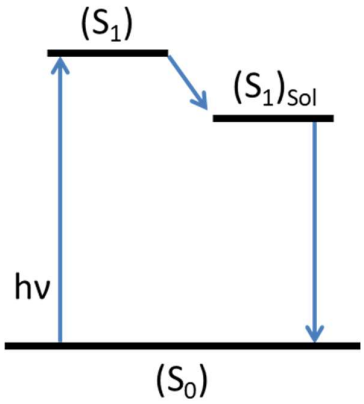

Figure S14. Fs-TAS (0 – 5.5 ns) of **DPP-Ph** in THF at room temperature: a) 3D fs-TAS obtained upon pump probe experiments following 430 nm laser excitation, b) respective time absorption profiles at the given wavelengths, c) deconvoluted fs-TAS spectra of the **DPP-Ph**-related singlet excited state (S_1) (black) and solvent stabilized singlet excited state $(S_1)_{Sol}$ (red) as obtained by target analysis using the proposed kinetic model shown in **Figure S12**, and d) respective population kinetics.

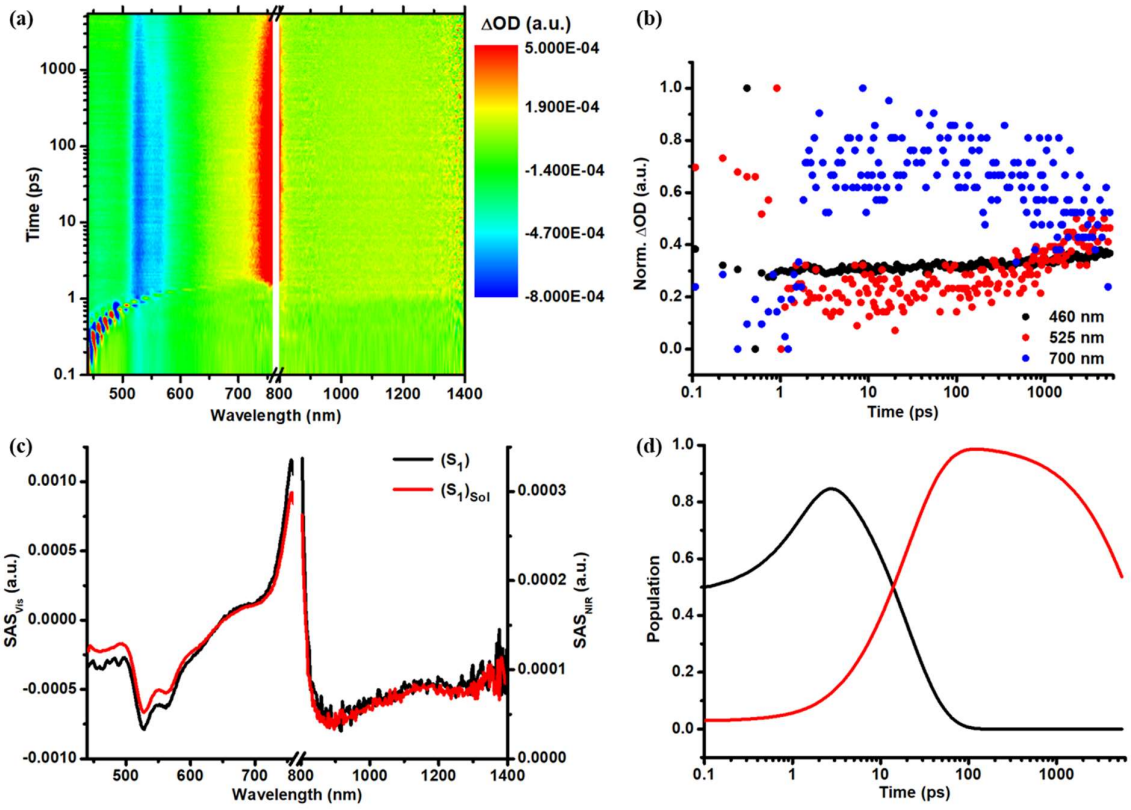

Figure S15. Ns-TAS (1 ns – 200 µs) of **DPP-Ph** in THF at room temperature: a) 3D ns-TAS obtained upon pump probe experiments following 430 nm laser excitation, b) respective time absorption profiles at the given wavelengths, c) deconvoluted ns-TAS spectra of the **DPP-Ph**-related solvent stabilized singlet excited state $(S_1)_{Sol}$ (red) as obtained by target analysis using the proposed kinetic model shown in **Figure S12**, and d) respective population kinetic.

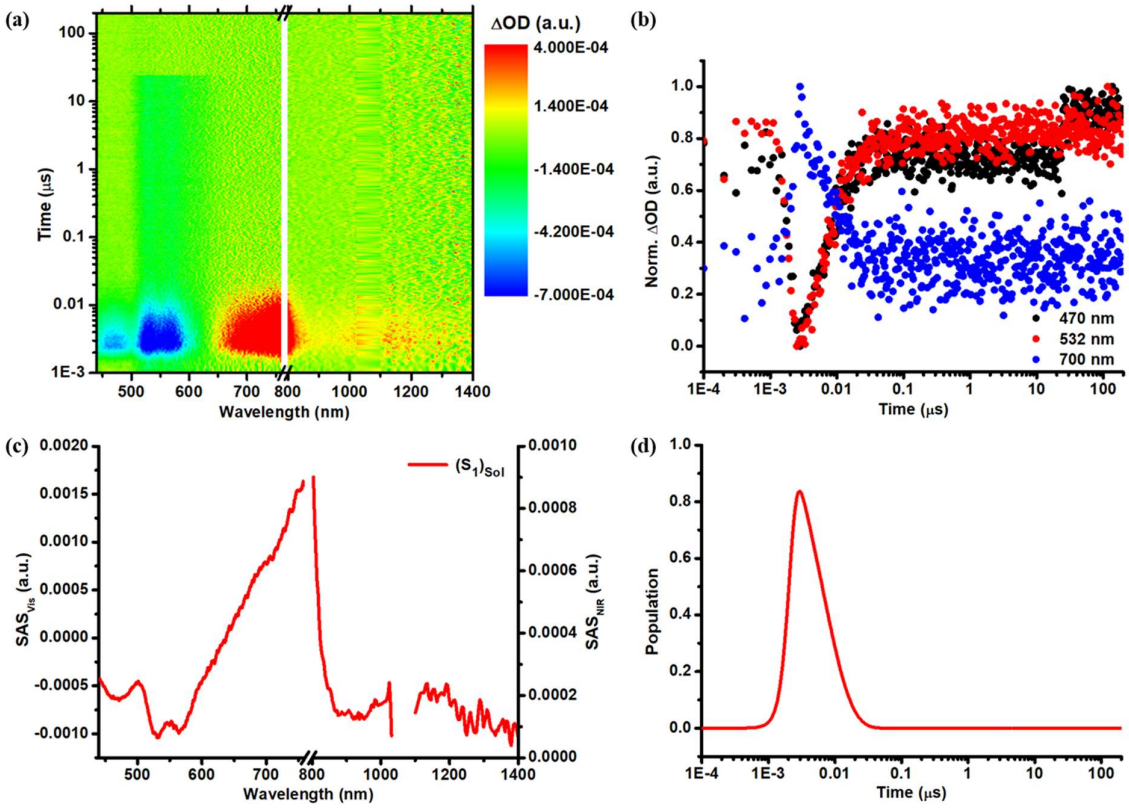

Figure S16. Ns-TAS (1 ns – 200 µs) of **DPP-Ph/SWCNT** in THF at room temperature: a) 3D ns-TAS obtained upon pump probe experiments following 430 nm laser excitation, b) respective time absorption profiles at the given wavelengths, c) deconvoluted ns-TAS spectra of the **DPP-Ph**-related solvent stabilized singlet excited state $(S_1)_{DPP2}$ (red) as obtained by target analysis using the proposed kinetic model shown in **Figure 8**, and d) respective population kinetic.

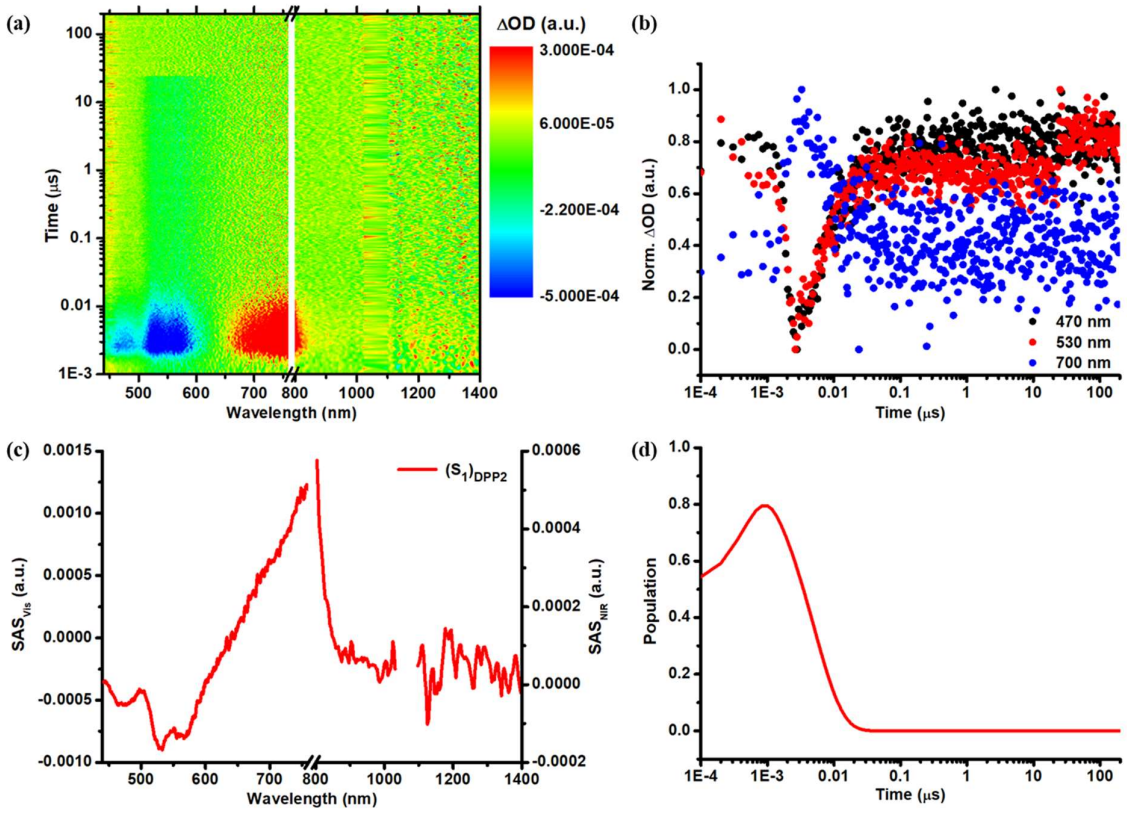

Figure S17. Fs-TAS (0 – 5.5 ns) of **DPP-PhBr** in THF at room temperature: a) 3D fs-TAS obtained upon pump probe experiments following 430 nm laser excitation, b) respective time absorption profiles at the given wavelengths, c) deconvoluted fs-TAS spectra of the **DPP-PhBr**-related singlet excited state (S_1) (black) and solvent stabilized singlet excited state $(S_1)_{Sol}$ (red) as obtained by target analysis using the proposed kinetic model shown in **Figure S12**, and d) respective population kinetics.

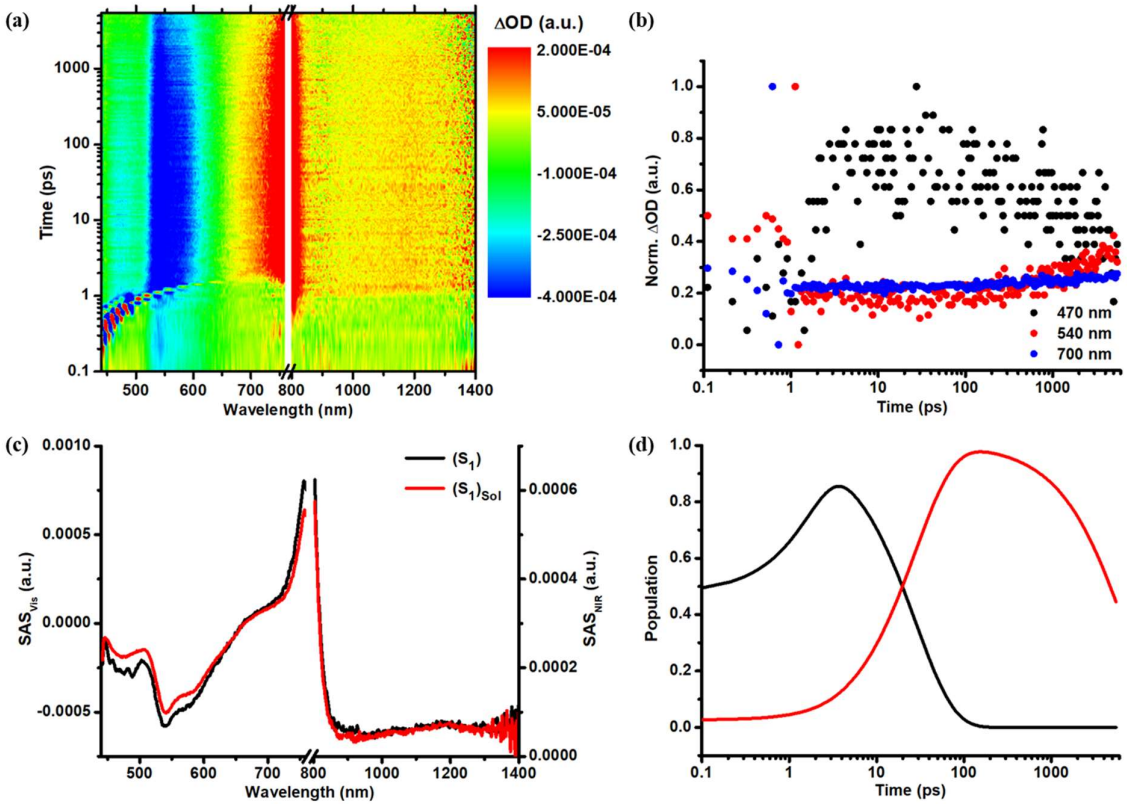

Figure S18. Ns-TAS (1 ns – 200 µs) of **DPP-PhBr** in THF at room temperature: a) 3D ns-TAS obtained upon pump probe experiments following 430 nm laser excitation, b) respective time absorption profiles at the given wavelengths, c) deconvoluted ns-TAS spectra of the **DPP-PhBr**-related solvent stabilized singlet excited state $(S_1)_{Sol}$ (red) as obtained by target analysis using the proposed kinetic model shown in **Figure S12**, and d) respective population kinetic.

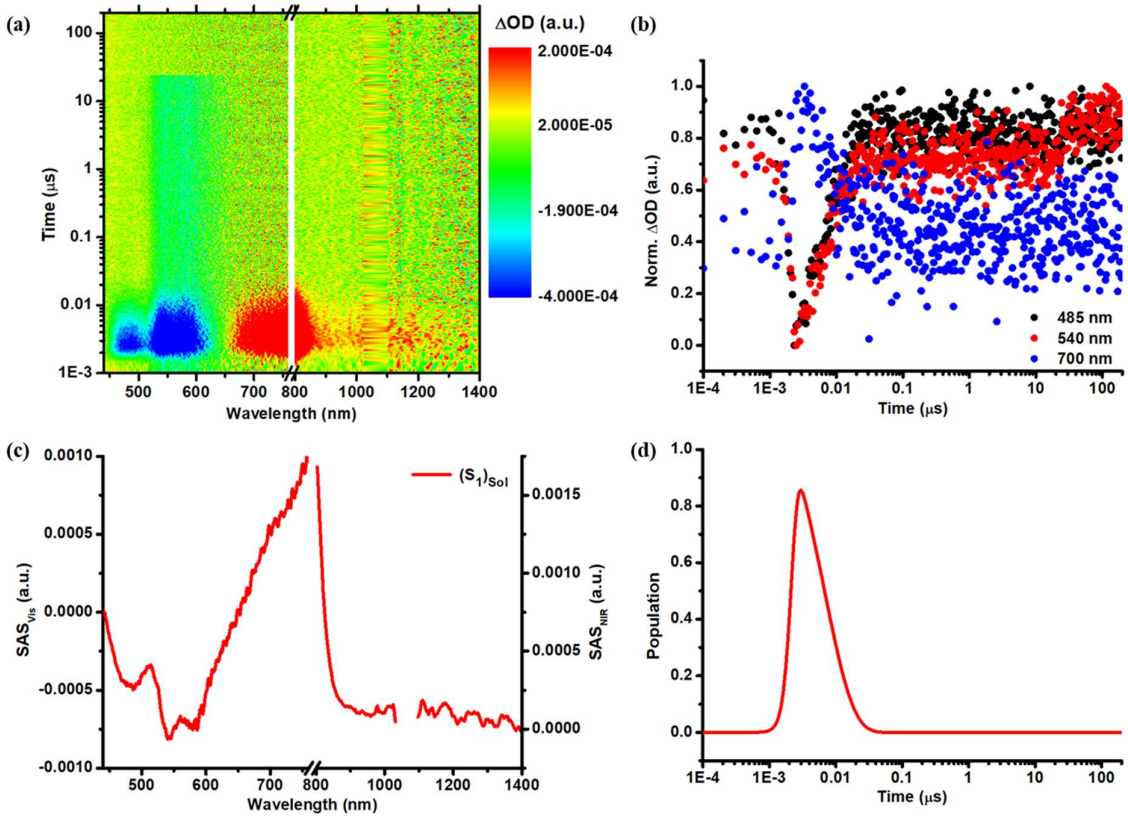

Figure S19. Fs-TAS (0 – 5.5 ns) of **DPP-PhBr/SWCNT** in THF at room temperature: a) 3D fs-TAS obtained upon pump probe experiments following 430 nm laser excitation, b) respective time absorption profiles at the given wavelengths, c) deconvoluted fs-TAS spectra of the SWCNT-related excited states $(S_1)_{NT1}$ (blue), $(S_1)_{NT2}$ (green), and $(S_1)^{CSS}_{NT3}$ (brown) and **DPP-PhBr**-related singlet excited state $(S_1)_{DPP1}$ (black) and solvent stabilized singlet excited state $(S_1)_{DPP2}$ (red) as obtained by target analysis using the proposed kinetic model shown in **Figure 8**, and d) respective population kinetics.

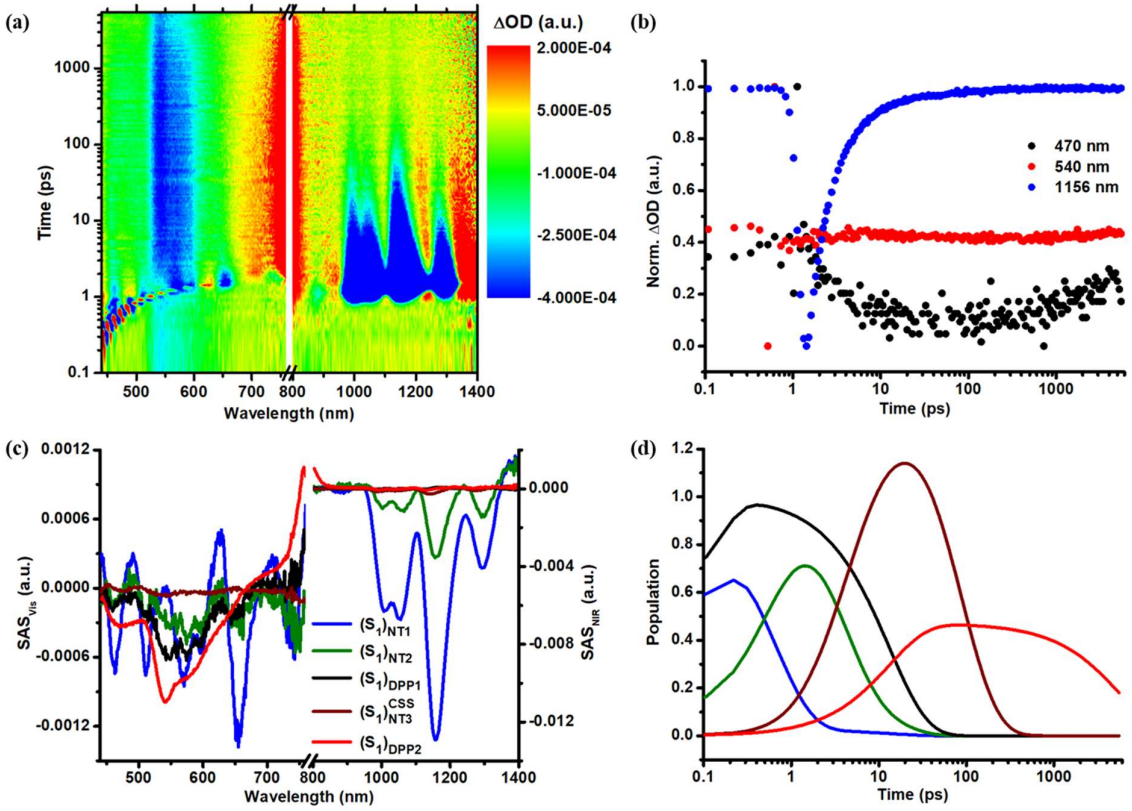

Figure S20. Ns-TAS (1 ns – 200 µs) of **DPP-PhBr/SWCNT** in THF at room temperature: a) 3D ns-TAS obtained upon pump probe experiments following 430 nm laser excitation, b) respective time absorption profiles at the given wavelengths, c) deconvoluted ns-TAS spectra of the **DPP-PhBr**-related solvent stabilized singlet excited state $(S_1)_{DPP2}$ (red) as obtained by target analysis using the proposed kinetic model shown in **Figure 8**, and d) respective population kinetic.

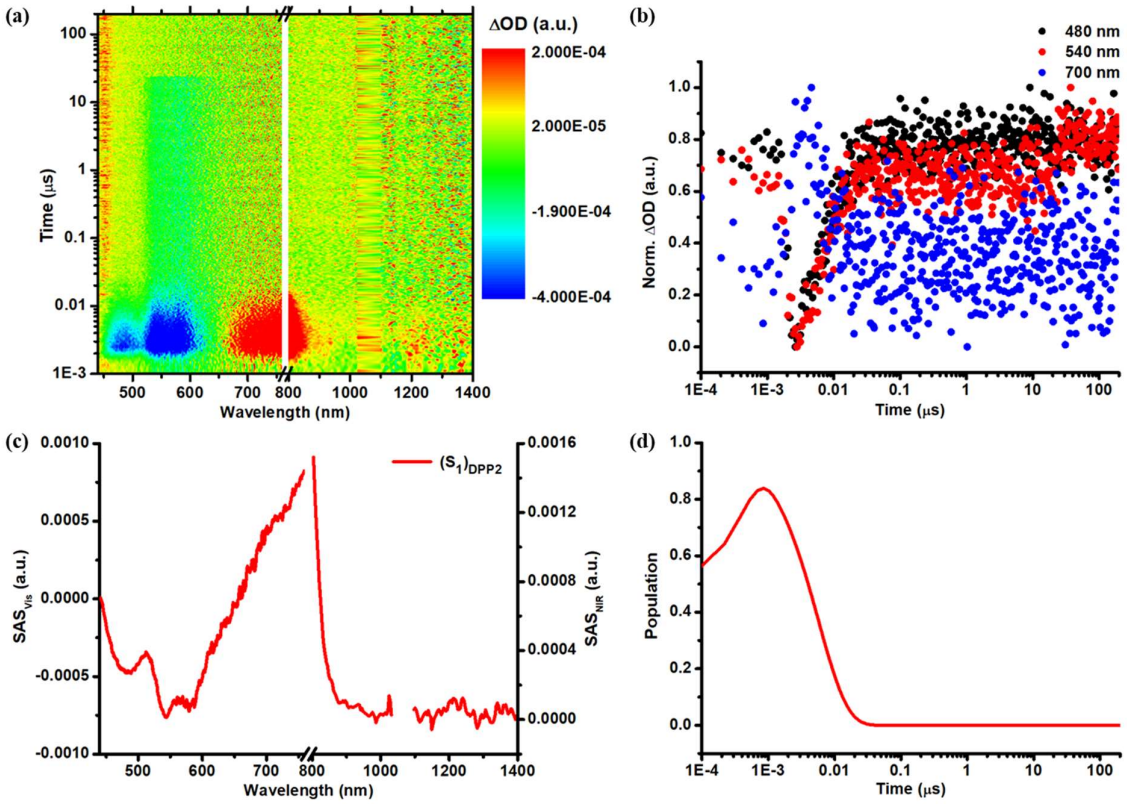

Figure S21. Fs-TAS (0 – 5.5 ns) of **DPP-Th** in THF at room temperature: a) 3D fs-TAS obtained upon pump probe experiments following 505 nm laser excitation, b) respective time absorption profiles at the given wavelengths, c) deconvoluted fs-TAS spectra of the **DPP-Th**-related singlet excited state (S_1) (black) and solvent stabilized singlet excited state $(S_1)_{Sol}$ (red) as obtained by target analysis using the proposed kinetic model shown in **Figure S12**, and d) respective population kinetics.

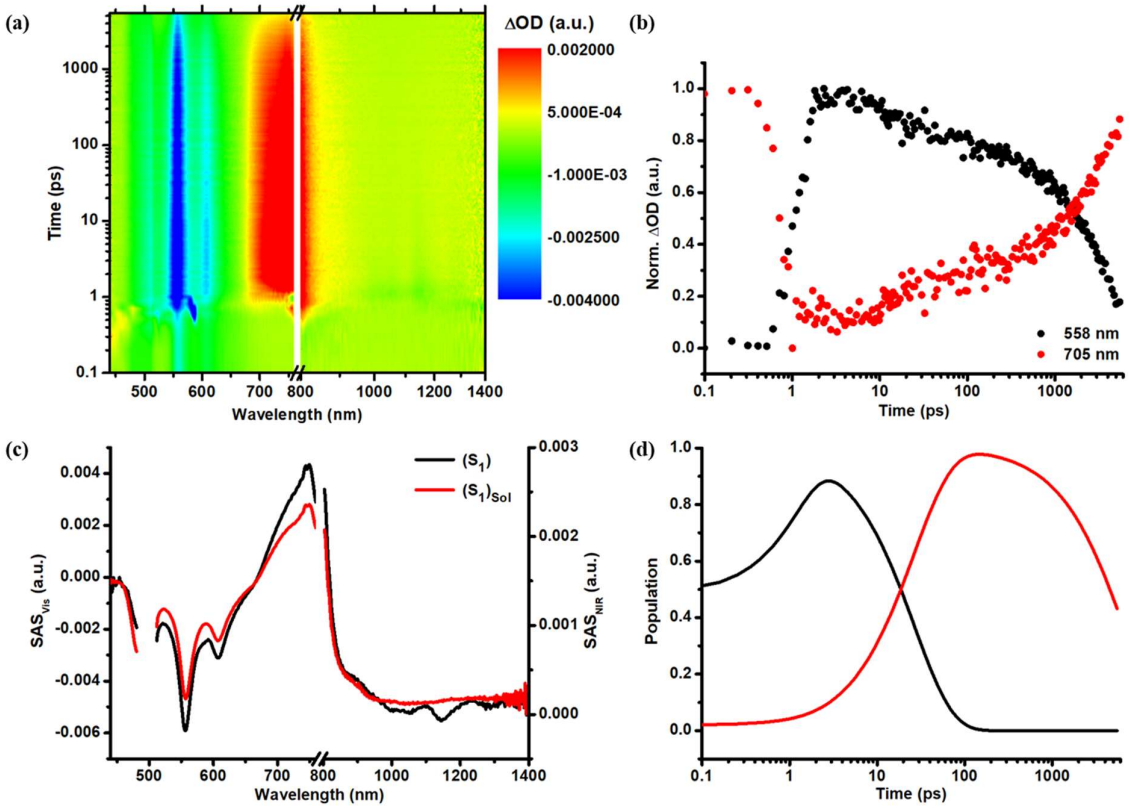

Figure S22. Ns-TAS (1 ns – 200 µs) of **DPP-Th** in THF at room temperature: a) 3D ns-TAS obtained upon pump probe experiments following 505 nm laser excitation, b) respective time absorption profiles at the given wavelengths, c) deconvoluted ns-TAS spectra of the **DPP-Th**-related solvent stabilized singlet excited state $(S_1)_{Sol}$ (red) as obtained by target analysis using the proposed kinetic model shown in **Figure S12**, and d) respective population kinetic.

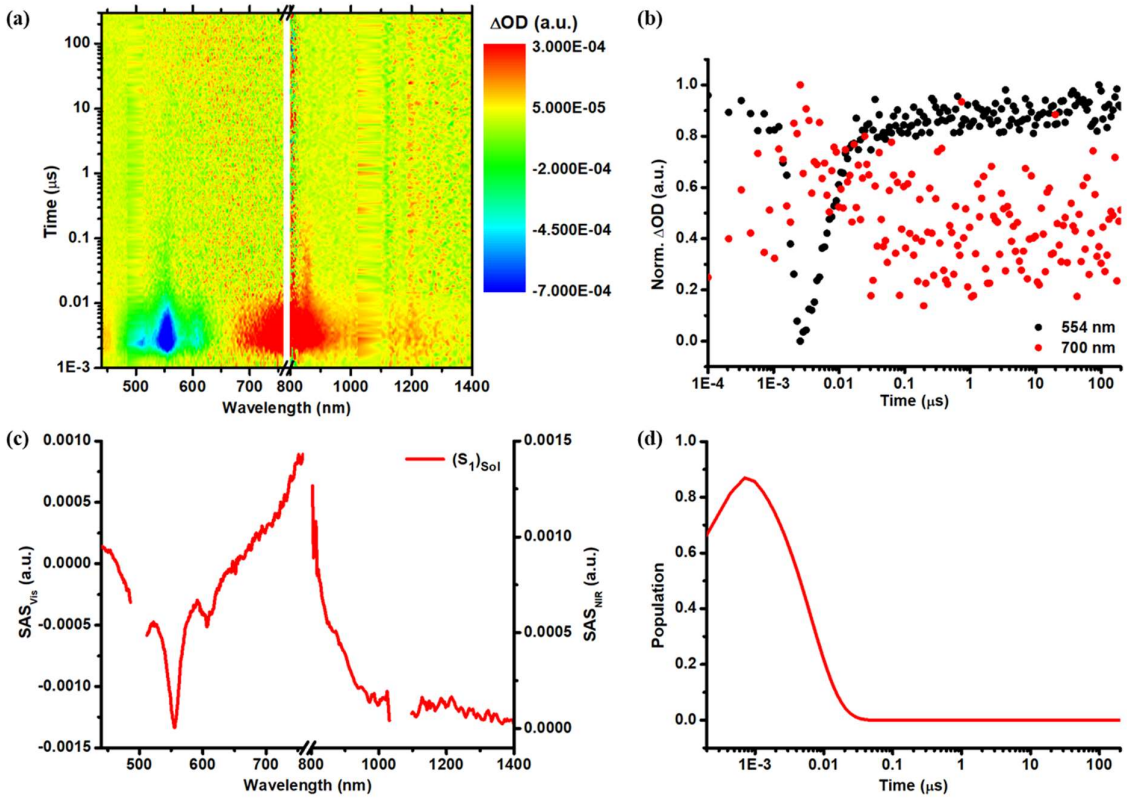

Figure S23. Fs-TAS (0 – 5.5 ns) of **DPP-Th/SWCNT** in THF: a) 3D fs-TAS obtained upon pump probe experiments following 430 nm laser excitation, b) respective time absorption profiles at the given wavelengths, c) deconvoluted fs-TAS spectra of the SWCNT-related excited states $(S_1)_{NT1}$ (blue), $(S_1)_{NT2}$ (green), and $(S_1)^{CSS}{}_{NT3}$ (brown) and **DPP-Th**-related singlet excited state $(S_1)_{DPP1}$ (black) and solvent stabilized singlet excited state $(S_1)_{DPP2}$ (red) as obtained by target analysis using the proposed kinetic model shown in **Figure 8**, and d) respective population kinetics.

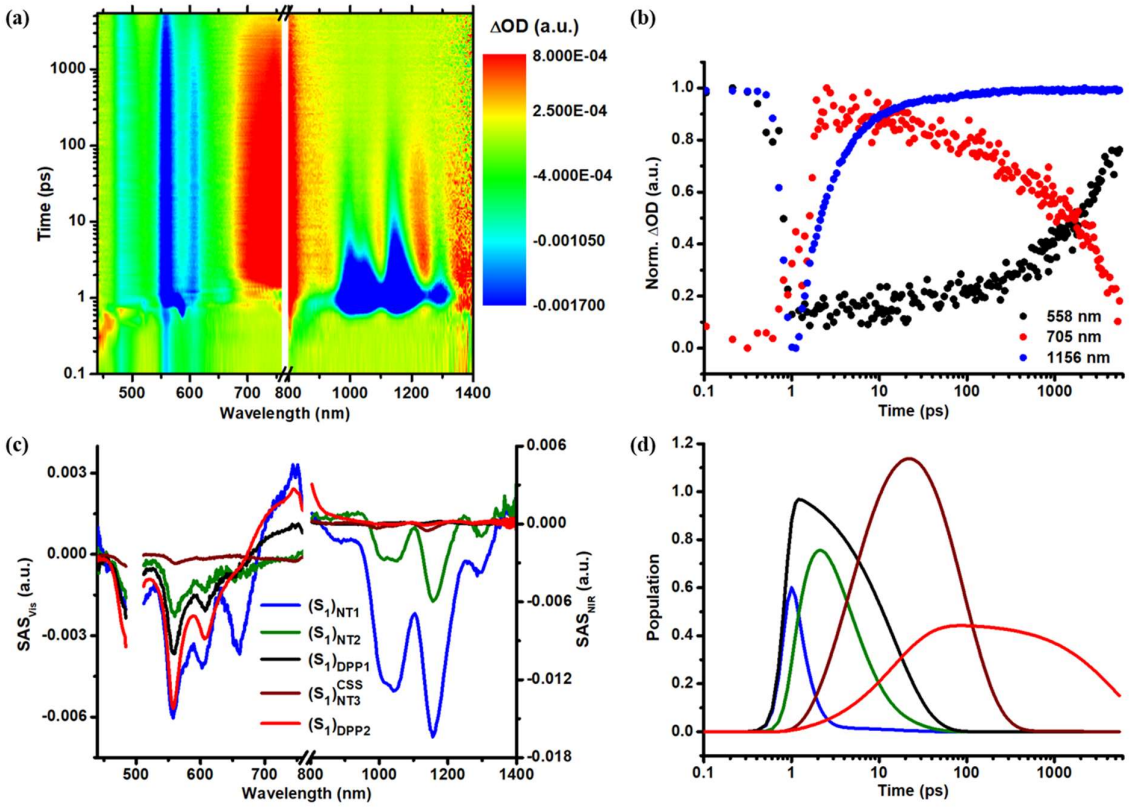

Figure S24. Ns-TAS (1 ns – 200 µs) of **DPP-Th/SWCNT** in THF: a) 3D ns-TAS obtained upon pump probe experiments following 430 nm laser excitation, b) respective time absorption profiles at the given wavelengths, c) deconvoluted ns-TAS spectra of the **DPP-Th**-related solvent stabilized singlet excited state $(S_1)_{DPP2}$ (red) as obtained by target analysis using the proposed kinetic model shown in **Figure 8**, and d) respective population kinetic.

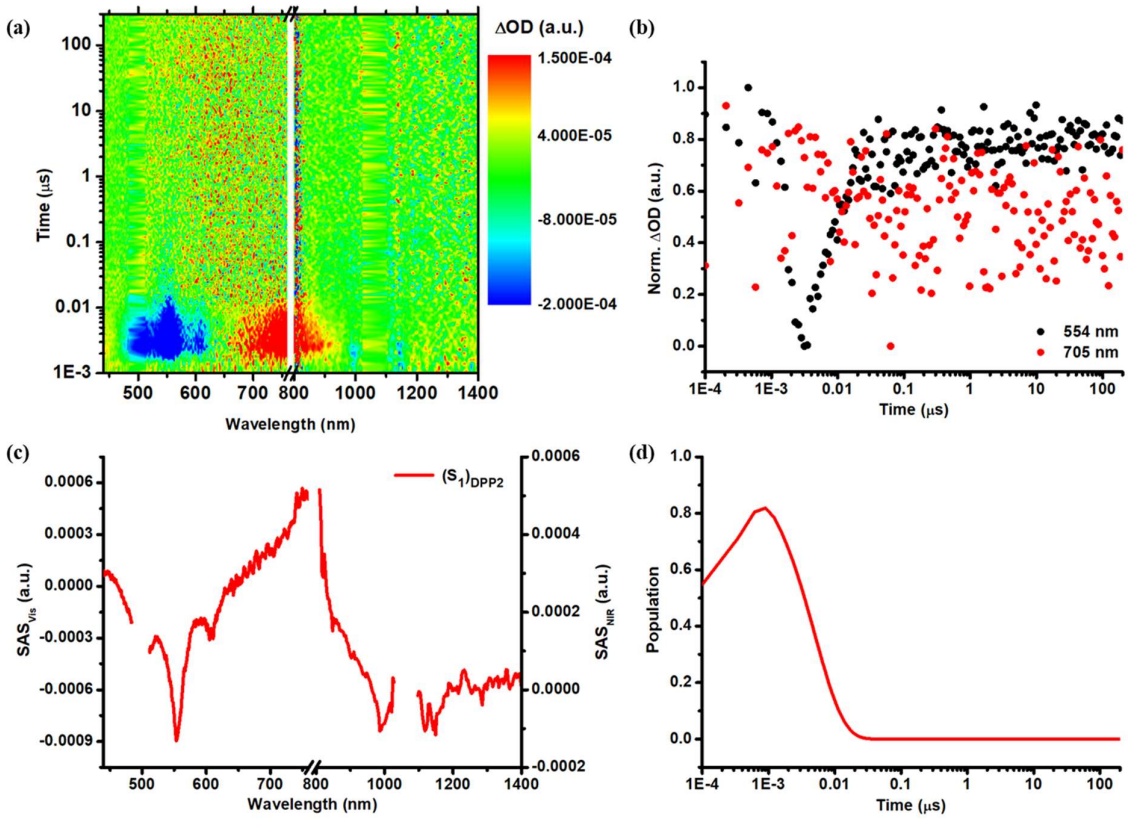

Figure S25. The apparent spectra of a) **DPP-Ph**, b) **DPP-PhBr**, and c) **DPP-Th** after subtraction of the differential absorption spectrum of SWCNT from **DPP-Ph/SWCNT**, **DPP-PhBr/SWCNT**, and **DPP-Th/SWCNT**, respectively in THF with corresponding SAS_{vis} $(S_1)_{NT3}$. The arrows show the presence of radical cation at ~675 nm.

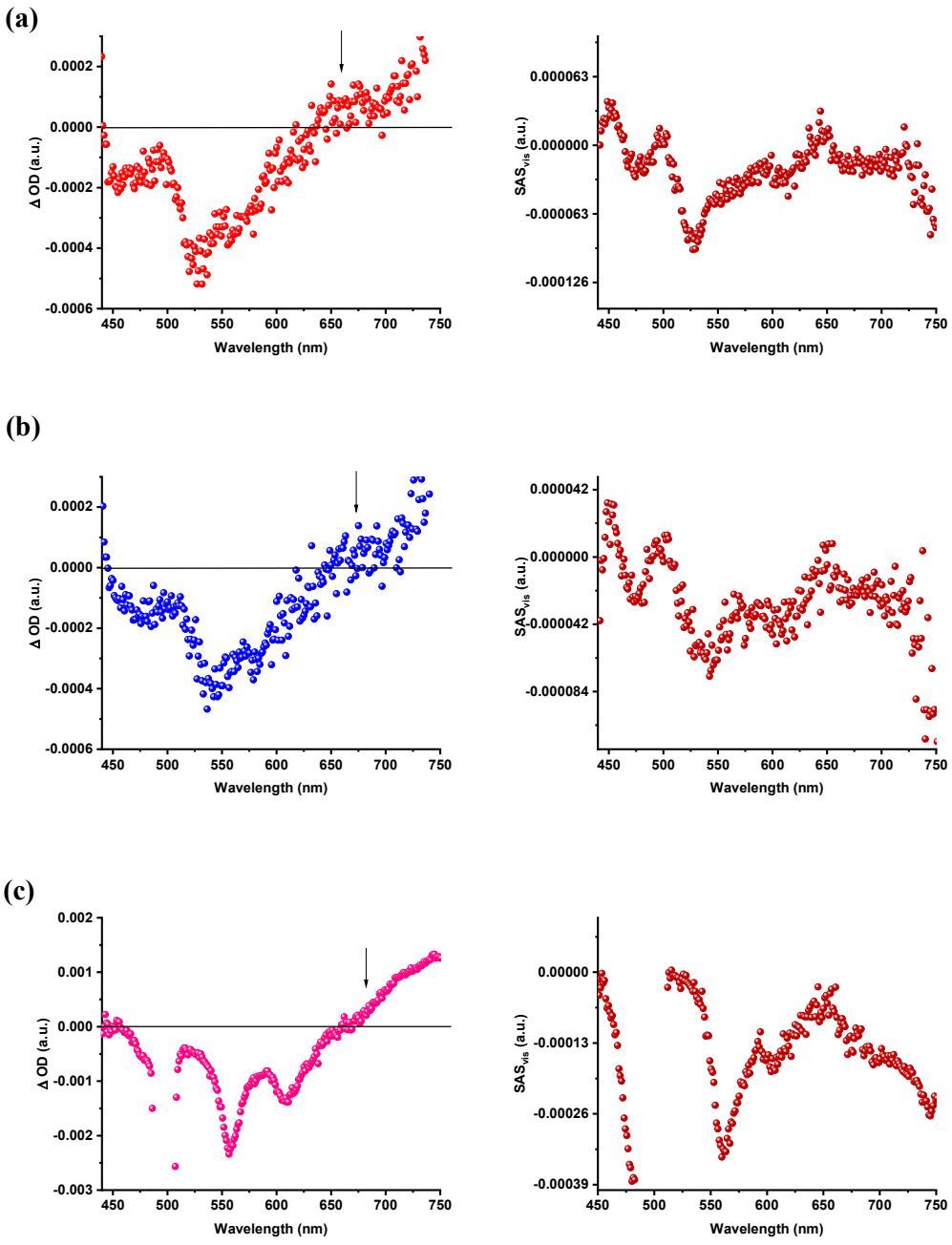

Pulse Radiolysis

The transient absorption spectra of the one-electron oxidized state of the DPP derivatives (**Figures S26-S28**) came from radiation chemical measurements, namely pulse radiolysis. The DPP samples were irradiated in N_2 saturated butyl chloride (n-BuCl) solutions with high-energy electron pulses (10 MeV, 15 ns duration, 85 Gy/pulse). Under these conditions the main reaction pathway includes the formation of radical cation of the DPPs (Equation S1, Equation S2):

$$\text{n-BuCl} \longrightarrow \text{n-BuCl}^{\bullet+} \qquad \text{(Equation S1)}$$

$$\text{n-BuCl}^{\bullet+} + \text{DPP} \rightarrow \text{n-BuCl} + \text{DPP}^{\bullet+} \qquad \text{(Equation S2)}$$

The broad transient maximum in the visible region between 300 and 900 nm after direct radiation is attributed to the $BuCl^{\bullet+}$ [2,3] and its decay goes hand-in-hand with the transient maxima of the formed $DPP^{\bullet+}$. Interestingly, transients which relate to the radical cation species of the diketopyrrolopyrrol moiety differ significantly when comparing **DPP-Ph** or **DPP-PhBr** with **DPP-Th**. For example, the transient absorption spectrum of **DPP-Ph**$^{\bullet+}$ gives rise to a transient absorption band in the UV with a maximum at 330 and broad transient absorption band in the visible between 510 and 800 nm with a maximum around 610 nm accompanied by transient absorption minimum at around 460 nm mirror imaging the ground state absorption (see Figure **S26a**). However, **DPP-Th**$^{\bullet+}$ demonstrates a transient absorption band in the UV and blue part of the optical spectrum with maxima at 360 and 420 nm, as well as a transient absorption in the red and NIR part with maxima at 600 and 860 nm. These transient absorption bands come along with a minimum 510 nm reflecting the ground state absorption of **DPP-Th** (see Figure **S28a**). The diversity between **DPP-Ph** or **DPP-PhBr** and **DPP-Th** in its radical cation transient absorption spectrum can be rationalized by their different peripheral moieties leading to the existence of different torsion angles, vibrionic states and, in consequence, electron density contributions.[4,5] The rate constants for the one electron oxidation of the DPP derivatives with n-BuCl$^{\bullet+}$ (Equation S2) were determined via analyses of the pseudo-first-order rate constants plotted vs. the concentrations of the DPP derivatives (see **Figures S26-S28**). Rate constants of 1.2×10^{10} $M^{-1}s^{-1}$ (**DPP-Ph**), 1.7×10^{10} $M^{-1}s^{-1}$ (**DPP-PhBr**), and 1.0×10^{10} $M^{-1}s^{-1}$ (**DPP-Th**) were derived from the linear relationships and are close to the diffusion limit.

Figure S26. (a) Pulse radiolysis spectrum of **DPP-Ph** in N_2 saturated n-BuCl, 500 ns after the electron pulse. The spectrum corresponds to the one-electron oxidized state of the diketopyrrolopyrrol derivative. (b) Corresponding time absorption profiles at 340 (black), 430 (green) and 540 nm (brown). The corresponding monoexponential global fit is depicted in cyan. (c) Plot of the pseudo-first-order rate constant versus **DPP-Ph** concentration.

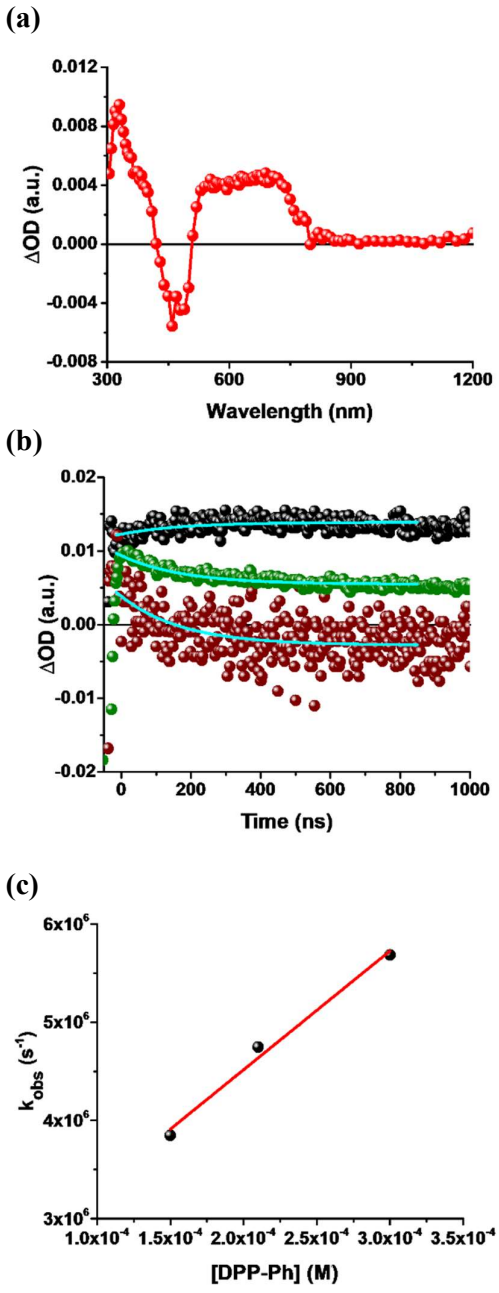

Figure S27. (a) Pulse radiolysis spectrum of **DPP-PhBr** in N_2 saturated n-BuCl, 500 ns after the electron pulse. The spectrum corresponds to the one-electron oxidized state of the diketopyrrolopyrrol derivative. (b) Corresponding time absorption profiles at 350 (black), 450 (dark green), 600 (brown), and 740 nm (light green). The corresponding monoexponential global fit is depicted in cyan. (c) Plot of the pseudo-first-order rate constant versus **DPP-PhBr** concentration.

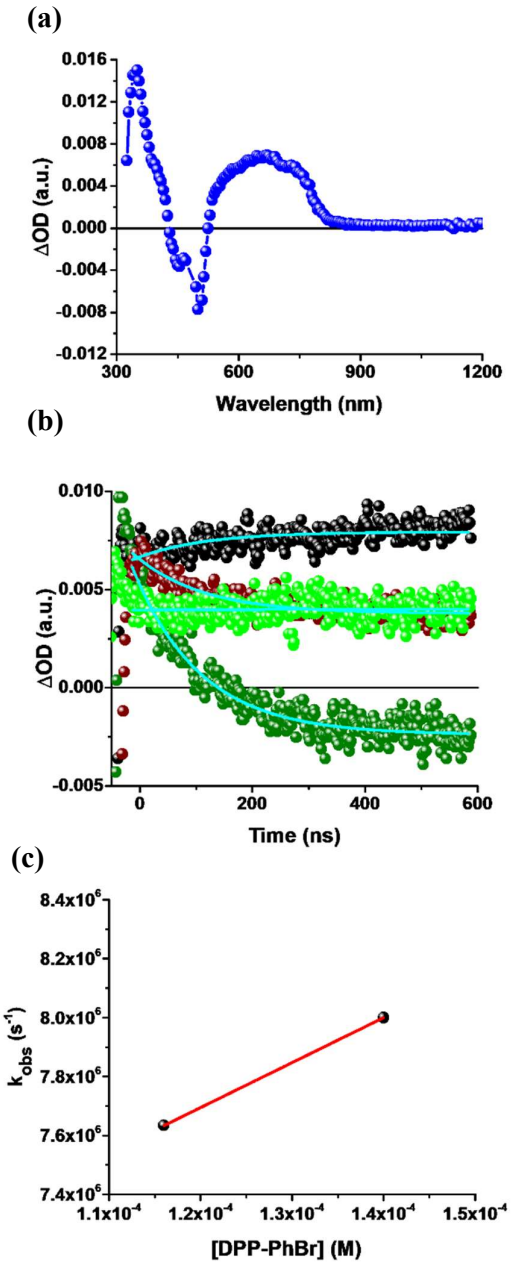

Figure S28. (a) Pulse radiolysis spectrum of **DPP-Th** in a N_2 saturated mixture of n-BuCl, 2 µs after the electron pulse. The spectra correspond to the one-electron oxidized state of the diketopyrrolopyrrol derivative. (b) Corresponding time absorption profiles at 450 (black), 570 (dark green), 640 (brown), 710 (light green), and 840 nm (orange). The corresponding monoexponential global fit is depicted in brown. (c) Plot of the pseudo-first-order rate constant versus **DPP-Th** concentration.

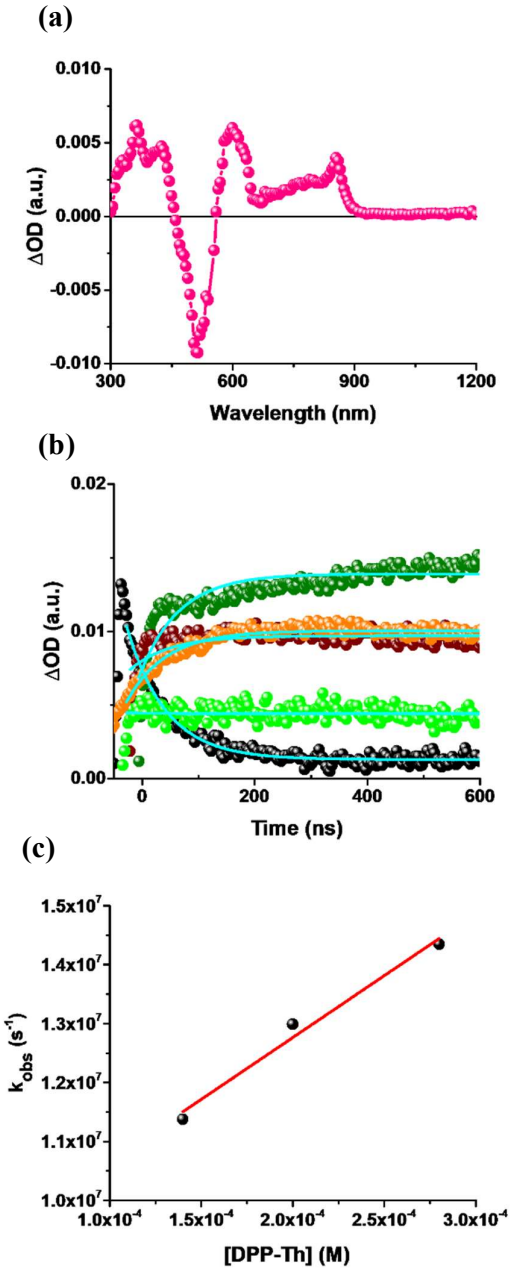

Supplementary References

1 J. H. Baxendale and F. Busi, Eds., *The Study of Fast Processes and Transient Species by Electron Pulse Radiolysis*, Springer Netherlands, Dordrecht, 1982.

2 S. Arai, A. Kira and M. Imamura, *J. Phys. Chem.*, 1976, **80**, 1968–1974.

3 R. Hermann, G. Ram Dey, S. Naumov and O. Brede, *Phys. Chem. Chem. Phys.*, 2000, **2**, 1213–1220.

4 M. Grzybowski and D. T. Gryko, *Adv. Opt. Mater.*, 2015, **3**, 280–320.

5 J. Dhar, N. Venkatramaiah, A. A. and S. Patil, *J. Mater. Chem. C*, 2014, **2**, 3457–3466.